PUC

Nota Científica 16/82

M-SUBSHELL IONIZATION OF Au, Pb, Bi, AND U BY PROTONS

N.V. de Castro Faria, F.L. Freire Jr., A.G. de Pinho

e A.F. da Silveira

DEPARTAMENTO DE FÍSICA

Outubro 1982

5.5

PONTIFÍCIA UNIVERSIDADE CATÓLICA DO RIO DE JANEIRO
DEPARTAMENTO DE FÍSICA
Rua Marquês de São Vicente, 225
Cx. Postal 38071 Telegramas: FISPUC
22453 Rio de Janeiro Brasil

Nota Científica 16/82

M-SUBSHELL IONIZATION OF Au, Pb, Bi, AND U BY PROTONS*

N.V. de Castro Faria, F.L. Freire Jr., A.G. de Pinho†
and E.F. da Silveira

Departamento de Física, Pontifícia Universidade Católica
Cx.P. 38071, Rio de Janeiro, RJ, Brasil

October 1982

ABSTRACT. M-subshell ionization cross sections of Au, Pb, Bi and U by protons bombardment were obtained over the projectile range 0.3 - 4.0 MeV. X-rays were detected by Si(Li) spectroscopy. At least one characteristic radiative transition line for each M-subshell was isolated and measured. Radiative and non-radiative branching ratios were taken from theoretical calculations of Bhalla and McGuire. Our total production X-ray cross-sections are compared with the measurements of other authors. Comparison of our scaled subshell ionization cross sections with calculations in the plane-wave Born approximation shows, in general, good agreement. Uncertainties in fluorescence yields and in super Coster-Kronig coefficients can introduce great imprecision in some experimentally determined subshell ionizations cross sections.

RESUMO. Foram medidas seções de choque de ionização das subcamadas M do Au, Pb, Bi e U por protons com energias entre 0.3 e 4.0 MeV. Essas medidas foram feitas a partir da análise de espectros dos raios-X emitidos pelos átomos após a ionização. Estes espectros foram obtidos com um detetor de Si(Li) de 190 eV de resolução à 5.9 keV (linha K_α do Fe) e cuidadosamente analisados por método gráfico desenvolvido no laboratório. As seções de choque de produção de raios-X M obtidas são comparadas com as de outros autores. Comparações entre as seções de choque experimentais de ionização das subcamadas e as calculadas na aproximação de Born de onda plana mostra em geral excelente concordância.

---

* Work partially supported by FINEP and CNPq.

† Present address: Institut de Physique Nucleaire de Lyon, 69622 Villeurbanne, France.

I. INTRODUCTION

During the last decade much progress has been made in the study of K and L-shell vacancies produced in heavy elements by MeV proton impact[1]. Otherwise, M shell studies are very scarce[2-5] due to experimental difficulties. Resolution is not so great a problem as a first look to a M x-ray spectrum obtained with Si(Li) spectroscopy seems to show. Groups of lines, where one or two transitions dominate, are isolated and extraction of a line representative of each subshell is possible (Fig. 1)

The measurement of efficiencies at the energies of M x-ray of heavy elements (~3 keV) is however a quite delicate problem. For high energies, experimental techniques are mandatory. In the energy region below 5 keV the scarcity of resolved lines from radiative sources and the uncertainty in the proton cross sections for K or L x-rays limit the accuracy of absolute efficiency measurements. The fact that at these energies the efficiency is essentially due to the exponential absorption of photons opens the possibility of using simple theoretical curves combined with experimental data.

As in the case of L-subshell studies, the knowledge of relative radiative decay rates, fluorescence yields and Coster-Kronig factors is another obstacle to calculate the ionization cross sections from the measured production x-ray cross sections. Precise and systematic measurements of these parameters are still lacking, and the use of theoretical calculations of Bhalla[6] and McGuire[7] is pratically the only

opened possibility.

M-subshell ionization cross sections in our region of interest has been calculated in the plane-wave Born approximation. Scaling of these values as a universal function for the 3s, 3p and 3d subshells for different values of θ and η/θ^2 is available[8] and can be compared with experimental results. An important aspect of these curves for the M_1 subshell is their double inflection that reflects the two non trivial nodes of the 3s electron wave functions. For the L_1 case[10,11], it is well known the correlation between the density node and the dominant impact parameter obtained from the approximate position of the observed plateau in the ionization cross sections vs energy curve.

The present work reports the measurements of the M-subshell and total X-rays production cross sections and the determination of the M-subshell ionization cross sections of Au, Pb, Bi and U for proton energies between 0.3 and 4.0 MeV. All relevant features mentioned in this introduction are analyzed and discussed in the text.

II. EXPERIMENTAL PROCEDURES AND ANALYSIS OF DATA

Thin targets (~5$\mu g/cm^2$) obtained by vacuum evaporation of Au, Pb and Bi onto Formvar, and of U onto Al, were employed in the experiments to avoid the need of large corrections of self-absorption of the x-rays. Beams of 0.3 to 4.0 MeV of protons were produced at the PUC/RJ Van de Graaff accelerator. Currents were kept below 30 nA to avoid pile-up effects.

The x-rays were detected by a Si(Li) detector with a measured resolution of 188 eV at 6.4 keV. The detector was positioned at 90° with respect to the beam and looked the target by reflection. Its sensitive volume was separated from the target by a Mylar window 6mm thick, air (17mm), beryllium (25μm), gold (200Å) and silicon dead layer (0,1μm). In the case of U target a Kapton foil (80μm) was introduced to eliminate the pile-up of the Al K x-rays with the $M_{\alpha\beta}$ line of U.

The M x-ray intensities were normalized to the simultaneously detected L_α x-ray lines from the same element avoiding therefore absolute measurements of the efficiency at low energies. In fact, precise measurements of the L_α production cross sections are now available[1,9-13]. Relative efficiencies between 2 and 13 keV were obtained by three different methods, namely, the K_α and K_β pairs of points, the K shell relative production cross sections and theoretical calculations.

The method of pair of points employs the well determined ratio between K_α and K_β lines[14]. Thin targets of elements with K x-rays in the region of interest were irradiated with protons of 2 MeV and the radiation detected in the same geometry as the actual experiments[10]. This technique is more useful when the K_α or K_β line of one element with atomic number Z falls between the K_α and K_β lines of the element with $Z \pm 1$, which happens for $Z \geq 23$. In all cases the pair of points gives the derivative of the efficiency curve in the corresponding K x-ray energy. Below about 3 keV, the method used was to irradiate with protons very thin films prepared with two different elements, one having K x-rays in the very low energy region and the other

higher than about 6 keV. For example, we prepared a target evaporating copper ($1\mu g/cm^2$) onto Formvar backing and aluminum ($1\mu g/cm^2$) onto the copper surface. The number of atoms was determined by detecting the protons elastically scattered at 90^o with respect to the beam direction and the x-ray simultaneously. The relative K x-rays production cross sections were taken from reference 15. Finally, the shape of the efficiency curve was obtained from theoretical calculations, with the thicknesses of the different absorption materials left as free parameters. The best fit to the experimental sets of points and derivatives changes very little the nominal values of the mylar and Kapton thicknesses, and it is not very sensitive to small changes in the thickness of the other absorption materials. We estimated the uncertainties of the overall efficiency factor, that is, the relative efficiency for our experimental set up, as being lesser than 10%.

It can be seen in Fig. 1 that we have three well defined groups of lines, the first dominated by the M_4N_6 and M_5N_7 transitions, the second by the M_3O_5 and M_2N_4 ones and the third by the M_2O_4 line and the complex cluster of lines $M_1O_{2,3}$ and $M_1P_{2,3}$. A peak fitting procedure had to be used to extract accurate values for the intensities of these lines. A graphical stripping method was employed and its description can be found in reference 10. For the determination of the M_4 and M_5 subshells ionization cross sections the lines of the first group, i.e., M_4N_6 and M_5N_7 could be selected and extracted with good precision in all the cases. The same thing occured for the M_3 subshell with the M_3O_5 transition, a line of the second-group. For energies

smaller than 1 MeV, M_1 and M_2 subshells were analysed from the lines $M_1O_{2,3}$, $M_1P_{2,3}$ and M_2O_4 of the third group, respectively. For higher energies, background coming from bremsstrahlung prevents the use of the lines of this group. We can still use the M_2N_4 line of the second group to get information about the M_2-ionization cross section. The theoretical radiative branching ratios[6] were used as a guide to the graphical stripping method.

III. RESULTS AND DISCUSSION

In Tables I to IV we present the experimental x-ray production cross sections of the selected lines representative of each M subshell, i.e., the areas of the M lines normalized to the L_α intensities and corrected for the L_α production cross sections and the global relative efficiency factor. All angular distributions of L and M x-rays were assumed to be isotropic . We assign an absolute standard deviation ranging from 15% for the M_1 group of lines to 11% for the M_4N_6 and M_5N_7 lines. They come mainly from the relative efficiency curve uncertainties, the statistical errors from counting being small.

To compare our measurements with available data in literature[2-5], we calculated the total M x-ray cross sections with the values of Tables I to IV and the theoretical radiative branching ratios of Bhalla[6]. The cross sections are presented in Fig. 2 together with the results of other authors. In fact, the data from references 2 to 5 were obtained taking average efficiencies for the first and second groups, the spectra not being decomposed into their components. When we use essentially the

same technique for our data, we obtained results differing by no more than 5% from our experimental points represented in the figures. The solid lines are theoretical calculations of the total production cross sections obtained with the plane wave Born approximation total ionization cross sections and average fluorescence coefficients defined in reference 7.

The ionization cross sections of each subshell can be written as explicit functions of the x-ray production cross sections, as shown in reference 8. With the fluorescence yields, the Coster-Kronig and super Coster-Kronig factors calculated by McGuire[7], we obtained the scaled ionization cross sections presented in Figures 3 to 7.

Calculations of M subshell ionization were performed by Johnson et al[8] in the plane-wave Born approximation and presented in the form of a scaled ionization cross section, the function $F_{3\ell}(\eta/\theta^2,\theta)$, where ℓ denotes the orbital angular momentum quantum number. The dimensionless parameters η and θ are the scaled incident energy and binding energy[16,17], respectively.

Total M-shell ionization cross sections were also obtained by the same authors starting from the ionization cross section of each of the five energy eigenstates, summing them with coefficients reflecting the statistical weight of the 3s, 3p and 3d electrons. Finally, with an average fluorescence coefficient[7], we obtained the total M x-ray production cross section. These cross section calculations reproduce very well our results (Fig. 2) showing the coherence of the data, particularly of the dominant lines M_4N_6 and M_5N_7 which are very little influenced by the

intensities of the transitions going to the M_1, M_2, and somewhat less, to the M_3 subshells.

The scaled ionization cross sections are presented in Figures 3 to 7. The experimental points concerning the M_1 subshell exhibt very clearly the plateau corresponding to the inner node of the radial 3s-wavefunction. To observe the outer node would require an impact energy too low for our accelerator. The inflection associated to the single nontrivial node of the 3p-wave function is much less pronounced. Agreement with the theoretical calculations is very poor for M_3 and M_5-subshells despite the fact that the $M_1O_{2,3}$, $M_1P_{2,3}$ and M_2O_4 or M_2N_4 are more difficult to be extracted from the spectra than the M_3O_5 or M_5N_7 line. With our data we are not able to give a definite explanation of this fact, but we can notice that a set of fluorescence yields and of super Coster-Kronig factors can be found that makes the data to agree well with the theoretical calculations in all the subshells. In fact, if we take the ratio between the ionization cross sections $\sigma_I^{M_3}/\sigma_I^{M_2}$ for experimental results and compare with the PWBA predictions one can observe that the ratio ω_3/ω_2 should be of the order of two, for all elements studied. Thus, if we multiply ω_3 by a factor about 2 and if ω_2 is also modified and reduced about 20%, our data become in good agreement with the theoretical curves, as is shown in Figure 8.

IV. SUMMARY AND CONCLUSIONS

We have measured the total M-shell x-rays production cross sections of Au, Pb, Bi and U by proton impact in the energy range 0.3 - 4.0 MeV. We also have presented the five subshells ionization cross section in the form of scaled cross sections that can be directly compared with the three universal functions

$F_{3\ell}(\eta/\theta^2,\theta)$ of the plane wave Born approximation.

As should be expected from the beginning, the PWBA furnishes a very satisfactory description of the M-shell ionization by energetic massive projectiles. The PWBA is usually corrected for three effects[17]: the relativistic effects on the electron wavefunctions, the retardation and deflection of the projectile by the Coulomb field of the target nucleus and the perturbation of the atomic states of the target by the projectile. However it would be incorrect to impute to any of these effects the discrepancies we observed between some experimental data and the PWBA predictions. From the three above mentioned effects only the last one, the binding effect, could be of some importance in the lower part of the region of energy that has been explored by us. The severe deviations from the PWBA results we observed mainly in the M_3 and M_5 cases are very probably due to our lack of knowledge of the exact values of the radiative and nonradiative partial widths. A particular problem seems to occur with the calculated[7] values of the fluorescence yields of the 3p-subshells. So for we know there are no experimental data on M_2 and M_3-subshell yields. We observed that the modification in the distribution of the p-shell total radiative yield between M_2 and M_3 that seems to be necessary to improve the experience-theory agreement is a larger ω_3 and a lower ω_2 than calculated by McGuire[7]. More experimental information about the mechanisms of creation and filling of M-subshell vacancies is requerid before more detailed conclusions can be brought forward.

REFERENCES

1. Proc. 2nd Int. Workshop on Inner Shell Ionization, Nucl. Instr. Meth. 192 (1982).

2. K. Ishii, S. Morita, H. Tawara, H. Kaji and T. Shiokawa, Phys. Rev. A11, 119 (1975).

3. C.E. Busch, A.B. Baskin, P.H. Nettles, S.M. Shafroth and A.W. Waltner, Phys. Rev. A7, 1601 (1973).

4. K. Sera, K. Ishii, A. Yamadera, A. Kuwako, M. Kamya, M. Sebata, S. Morita and T.C. Chu, Phys. Rev. A22, 2536 (1980).

5. M. Sarkar, H. Mommsen, W. Sarter and P. Schürkes, J. Phys. B: Atom. Mol. Phys. 14, 3163 (1981).

6. C.P. Bhalla, J. Phys. B: Atom. Mol. Phys. 3, 916 (1970).

7. E.J. McGuire, Phys. Rev. A5, 1043 (1972).

8. D.E. Johnson, G. Basbas and F.D. McDaniel, Atom. Data and Nucl. Data Tables 24, 1 (1979) and IEEE Transactions on Nuclear Science, NS-26, 1162 (1979).

9. R.C. Bearse, D.A. Close, J.J. Malanify and C.J. Umbarger, Phys. Rev. A7, 1269 (1973).

10. C.V. Barros Leite, N.V. de Castro Faria and A.G. de Pinho, Phys. Rev. A15, 943 (1977`.

11. E.L.B. Justiniano, A.A.G. Nader, N.V. de Castro Faria, C.V. Barros Leite and A.G. de Pinho, Phys. Rev. A21, 73 (1980).

12. D. Bhattacharya, S.K. Bhattacherjee and S.K. Mitra, J. Phys. B: Atom. Mol. Phys. 13, 967 (1980).

13. W. Sarter, H. Mommsen, M. Sarkar, P. Schürkes and A. Weller, J. Phys. B: At. Mol. Phys. 14, 2843 (1981).

14. S.I. Salem, S.L. Panossian and R.A. Krause, Atom. Data and Nucl. Data Tables 14, 91 (1974).

15. S.A.E. Johansson and T.B. Johansson, Nucl. Instr. Meth. 137, 473 (1976).

16. E. Merzbacher and H.W. Lewis, Handbuch der Physik (Springer, Berlin) 34, 166 (1958).

17. G. Basbas, W. Brandt and R.M. Laubert, Phys. Rev. A7, 938 (1973).

Table Captions

Table I - X-ray production cross sections (in barns) of selected lines representative of gold M-subshells.

Table II - The same that Table I, for lead.

Table III - The same that Table I, for bismuth.

Table IV - The same that Table I, for uranium.

FIGURE CAPTIONS

Fig. 1 - M x-ray spectrum of U produced by 0.3 MeV protons. Also shown the selected transition lines representative of each M-subshell (solid curves), obtained after subtraction of the background and decomposition of the spectrum.

Fig. 2 - Experimental total M x-ray production cross section for Au, Pb, Bi and U. Also presented: PWBA theoretical curves.

Fig. 3 - Scaled experimental M_1 ionization cross section for Au, Pb, Bi and U. Also presented: PWBA theoretical curves for two different values of θ.

Fig. 4 - The same that Fig. 3, for M_2.

Fig. 5 - The same that Fig. 3, for M_3.

Fig. 6 - The same that Fig. 3, for M_4.

Fig. 7 - The same that Fig. 3, for M_5.

Fig. 8 - Scaled experimental M_3, M_4 and M_5 ionization cross sections calculated with the modified ω_3 and ω_2. Also presented: PWBA theoretical curves for two different values of θ.

TABLE I

Energy (MeV)	M_5N_7	M_4N_6	M_3O_5	M_2N_4	$M_1O_{2,3}^{+}$ $M_1P_{2,3}$
0.3	69.9	37.3	0.21	0.25	0.024
0.4	117.6	77.3	0.46	0.52	0.051
0.5	196.0	126.9	0.91	1.04	0.067
0.6	240.6	157.6	1.44	1.52	0.12
0.7	273.9	179.5	1.78	2.00	0.17
0.8	370.2	209.6	2.55	3.27	0.26
0.9	471.9	193.6	3.20	3.27	0.41
1.0	418.9	309.2	4.35	4.88	0.50
1.2	533.5	341.2	5.01	6.02	0.57
1.4	622.6	369.9	5.40	8.52	0.63
1.6	648.7	508.6	7.21	11.3	0.82
1.8	729.5	600.3	8.57	14.1	1.18
2.0	714.4	710.4	9.46	13.9	1.31
2.2	711.6	763.8	9.95	16.0	1.48
2.4	707.9	778.7	11.49	16.8	1.70
2.6	884.8	766.3	11.56	17.2	1.72
2.8	864.9	775.9	11.24	17.4	1.74
3.0	924.0	875.4	13.00	23.1	1.66
3.2	1021.0	848.0			
3.4	1027.0	845.5			
3.6	1063.7	861.2			
3.8	1037.7	853.9			
4.0	1042.1	874.3			

TABLE II

Energy (MeV)	M_5N_7	M_4N_6	M_3N_5	M_3O_5	M_2N_4	$M_1O_{2,3}$+ $M_1P_{2,3}$
0.3	45.5	18.7	1.66	0.14	0.14	0.022
0.4	82.4	37.5	3.72	0.32	0.30	0.035
0.5	129.8	57.2	7.83	0.67	0.55	0.059
0.6	168.2	72.5	12.3	1.08	0.83	0.098
0.7	208.1	93.6	17.9	1.56	1.20	0.14
0.8	264.9	130.0	28.7	2.51	1.92	0.21
0.9	270.9	134.6	29.9	2.57	1.99	0.24
1.0	346.2	170.1	44.8	3.83	2.81	0.37
1.2	414.7	198.8	61.3	5.33	4.08	
1.4	503.1	257.3	85.5	7.23	5.08	
1.6	583.8	282.4	110.4	9.57	6.68	
1.8	627.6	315.6	126.4			
2.0	708.9	386.1	163.8			
2.2	728.6	442.6	173.0			
2.4	782.2	465.8	193.6			
2.6	879.2	562.1	219.8			
2.8	845.7	549.3	204.7			
3.0	935.8	563.6	210.2			
3.2	904.1	575.8	218.2			
3.4	903.7	580.1	227.6			
3.6	895.7	568.2	224.9			
3.8	880.7	563.1	206.8			
4.0	856.9	556.6	208.3			

TABLE III

Energy (MeV)	M_5N_7	M_4N_6	M_3O_5	M_2N_4	$M_1O_{2,3}$+ $M_1P_{2,3}$
0.3	46.9	12.2	0.17	0.17	0.021
0.4	69.4	35.4	0.30	0.33	0.030
0.5	118.3	58.7	0.69	0.55	0.048
0.6	154.5	78.9	0.97	0.95	0.067
0.7	202.4	100.8	1.71	1.43	0.11
0.8	243.5	92.9	2.16	2.09	0.18
0.9	295.7	158.4	2.91	2.62	0.27
1.0	333.0	194.3	3.58	3.70	0.33
1.2	446.5	242.2	5.64	5.87	0.51
1.4	547.4	294.6	7.11	8.10	0.86
1.6	601.3	316.4	8.77	9.10	1.02
1.8	673.0	357.8	11.0	9.66	1.53
2.0	692.5	427.8	13.0	11.3	
2.2	735.6	482.7	12.5	14.2	
2.4	758.5	493.5	13.3	15.0	
2.6	781.2	524.7	13.8	15.5	
2.8	836.8	536.5	14.5	17.7	
3.0	824.3	531.2	12.7	18.2	

TABLE IV

Energy (MeV)	M_5N_7	M_4N_6	M_3O_5	M_2N_4	M_2O_4	$M_1O_{2,3}^{+}$ $M_1P_{2,3}$
0.3	19.7	10.2	0.61	0.068	0.019	0.014
0.4	30.2	15.8	1.04	0.10	0.029	0.019
0.5	56.9	31.3	2.18	0.19	0.054	0.046
0.6	80.7	44.0	3.48	0.35	0.10	0.049
0.7	94.3	53.6	4.86	0.43	0.12	0.061
0.8	111.9	63.4	6.55	0.52	0.18	0.083
0.9	128.8	73.5	8.66	0.69	0.20	0.090
1.0	144.0	79.2	10.0	0.99	0.28	0.13
1.2	181.3	100.3	13.6	1.45	0.36	
1.4	191.3	122.4	21.6	2.16		
1.6	218.3	146.6	28.9	2.57		
1.8	255.1	168.9	33.6	3.23		
2.0	311.2	191.0	38.9	3.93		
2.2	348.1	212.2	45.1	4.74		
2.4	359.7	228.8	48.4	5.78		
2.6	455.8	234.5	53.0	7.04		
2.8	495.6	257.1	56.7	8.97		
3.0	493.3	255.9	56.6	8.09		

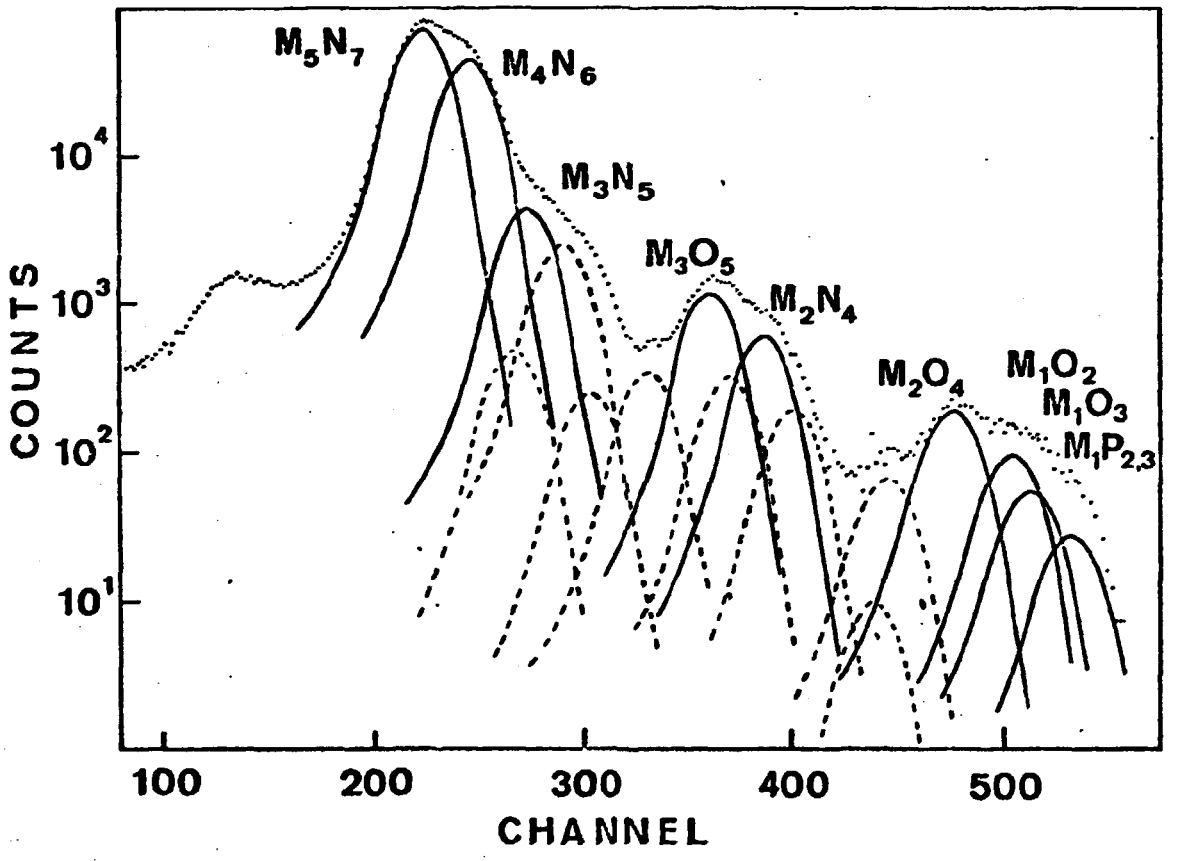
M5N7
M4N6
M3N5
M3O5
M2N4
M2O4
M1O2
M1O3
M1P2,3
10^4
10^3
10^2
10^1
COUNTS
100
200
300
400
500
CHANNEL

Figure 1

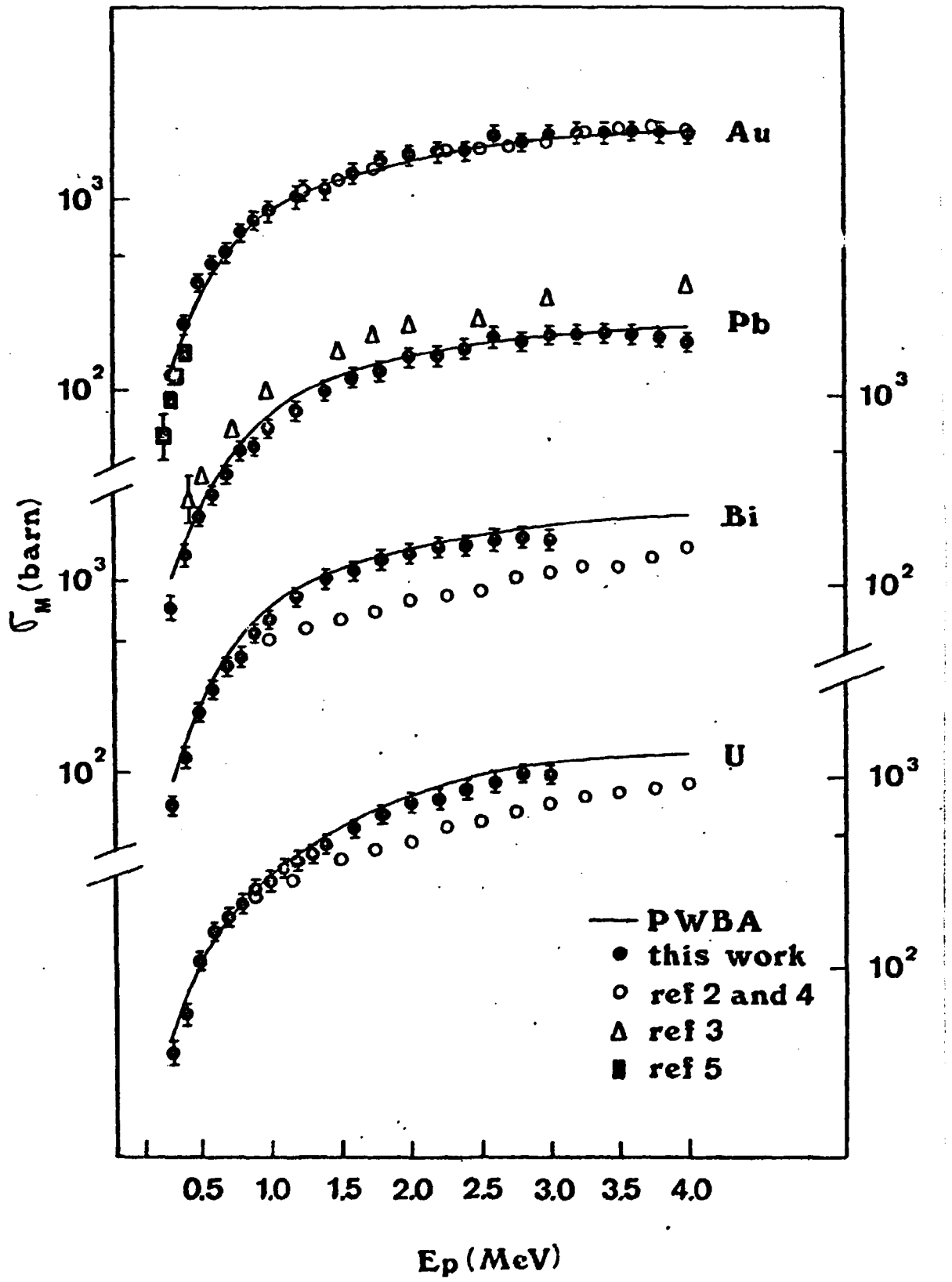
Au
Pb
Bi
U
PWBA
this work
ref 2 and 4
ref 3
ref 5
σ_M (barn)
Ep (MeV)
0.5
1.0
1.5
2.0
2.5
3.0
3.5
4.0
10^3
10^2

Figure 2

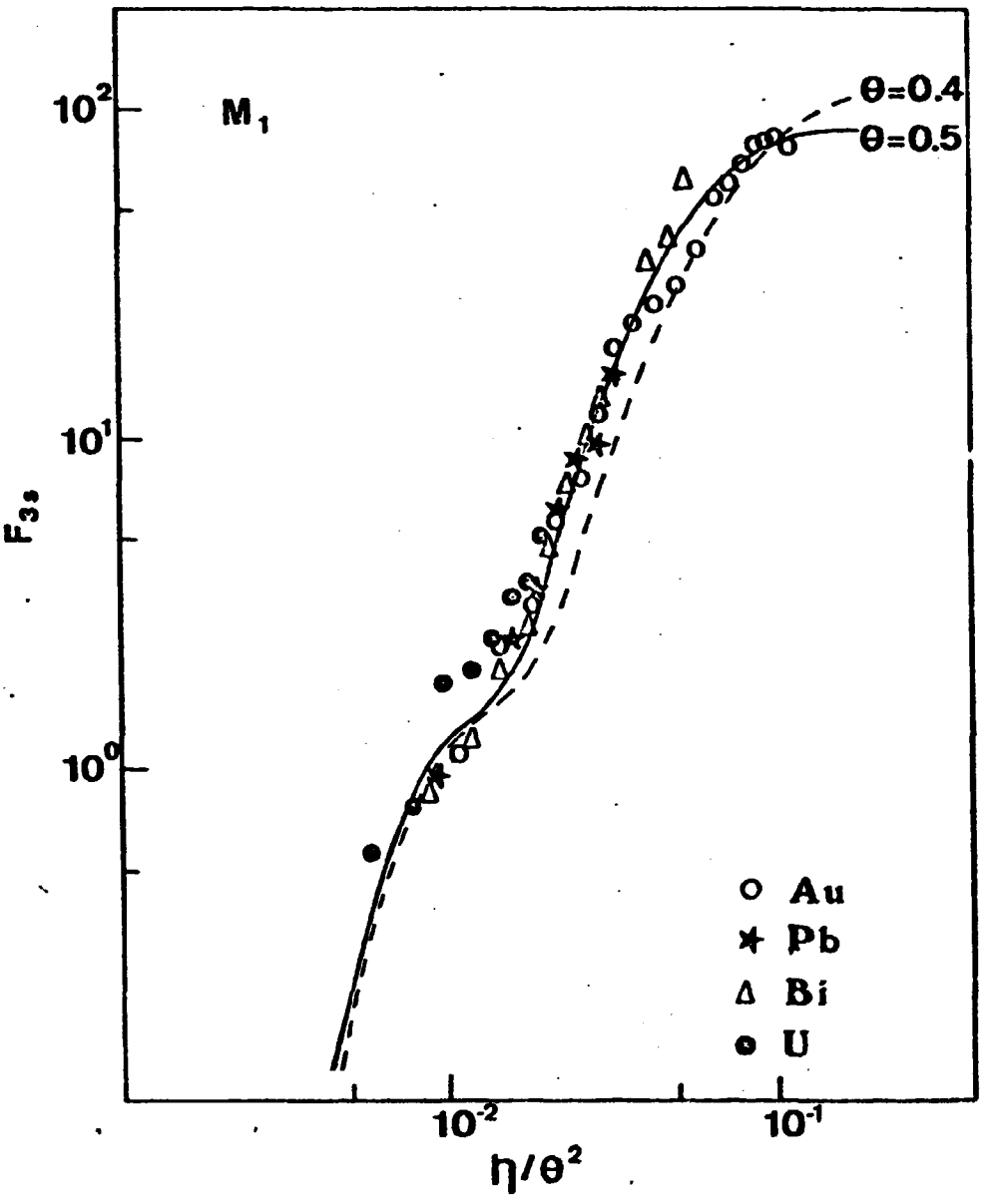

Figure 3

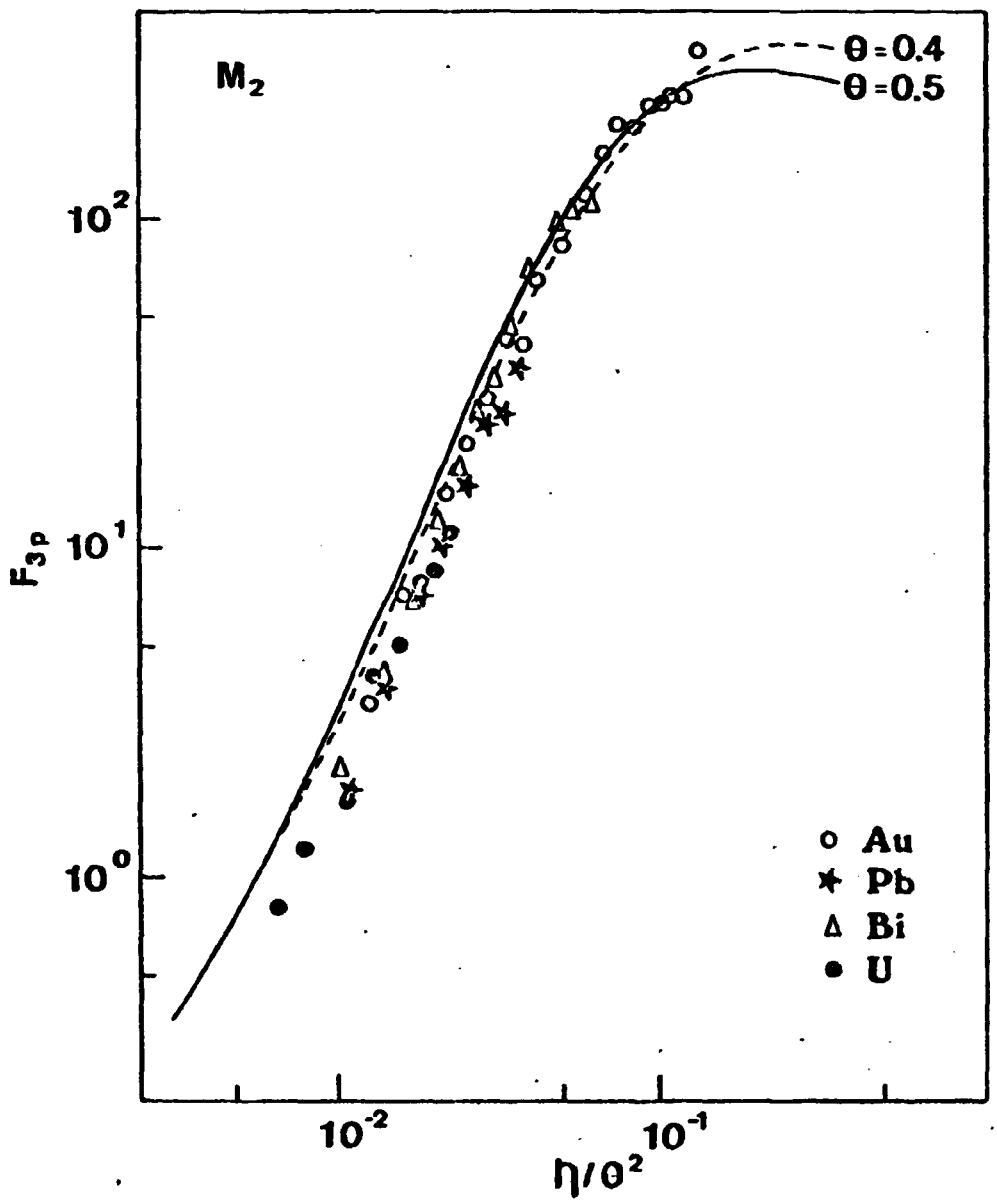

Figure 4

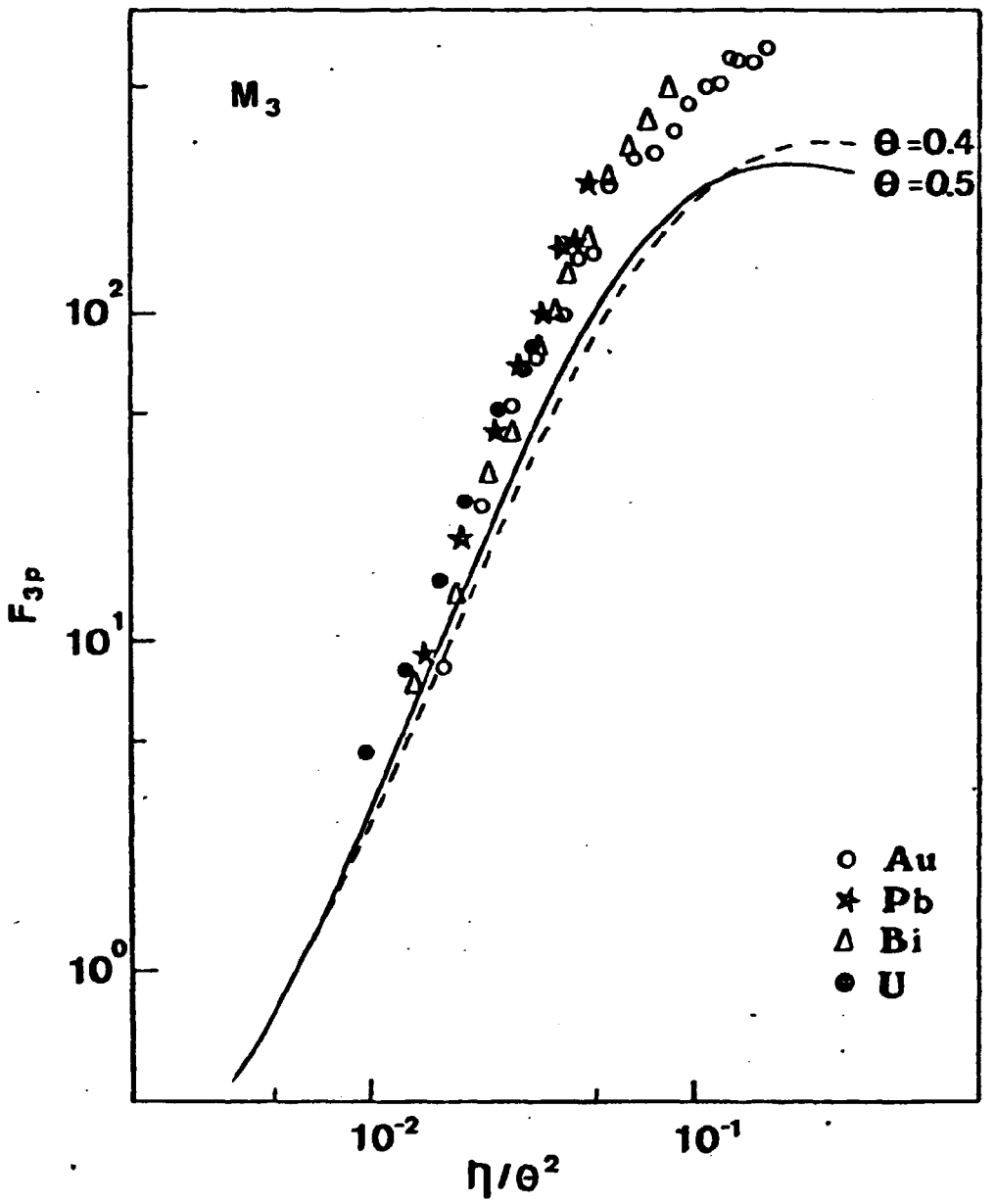

Figure 5

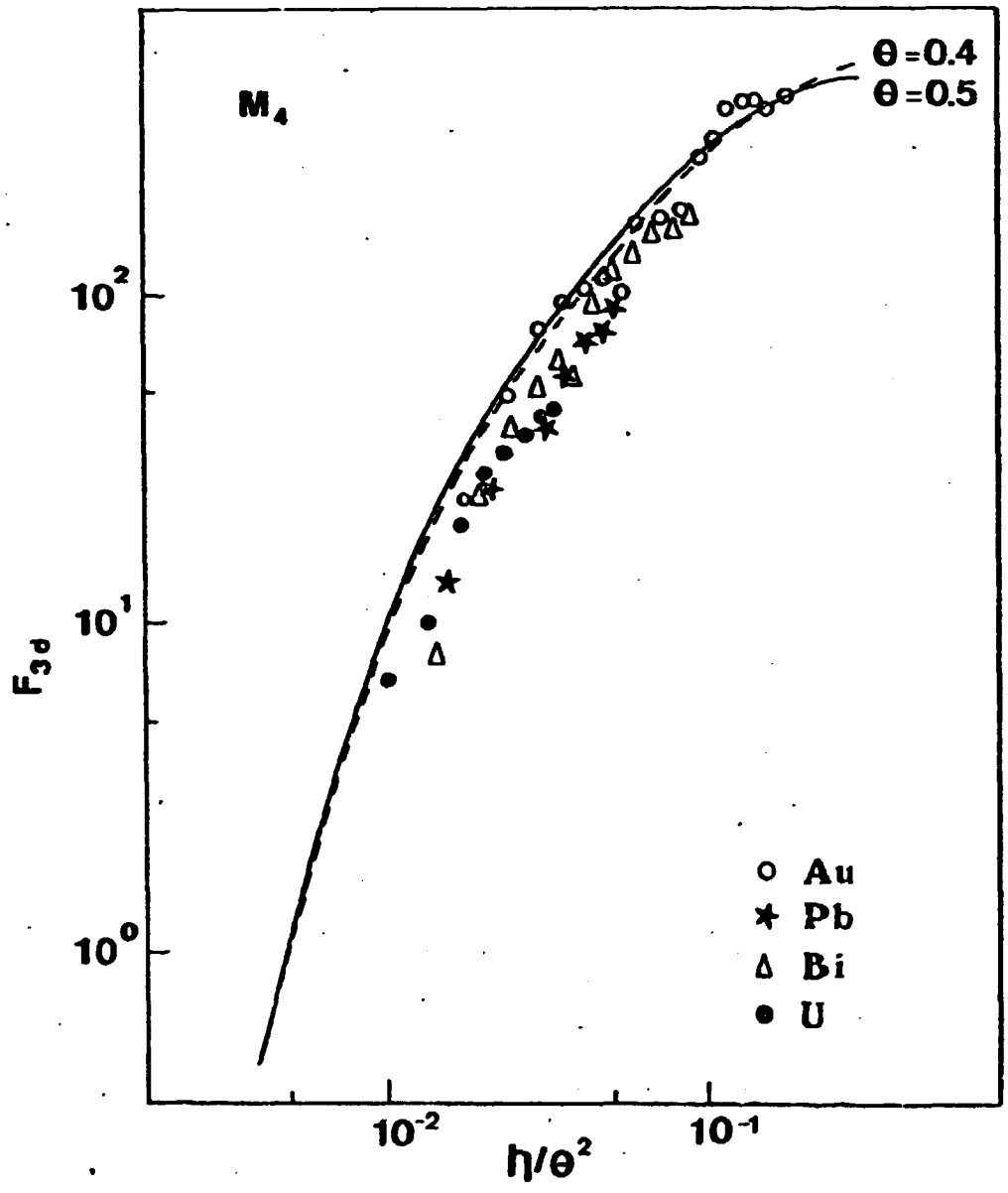

Figure 6

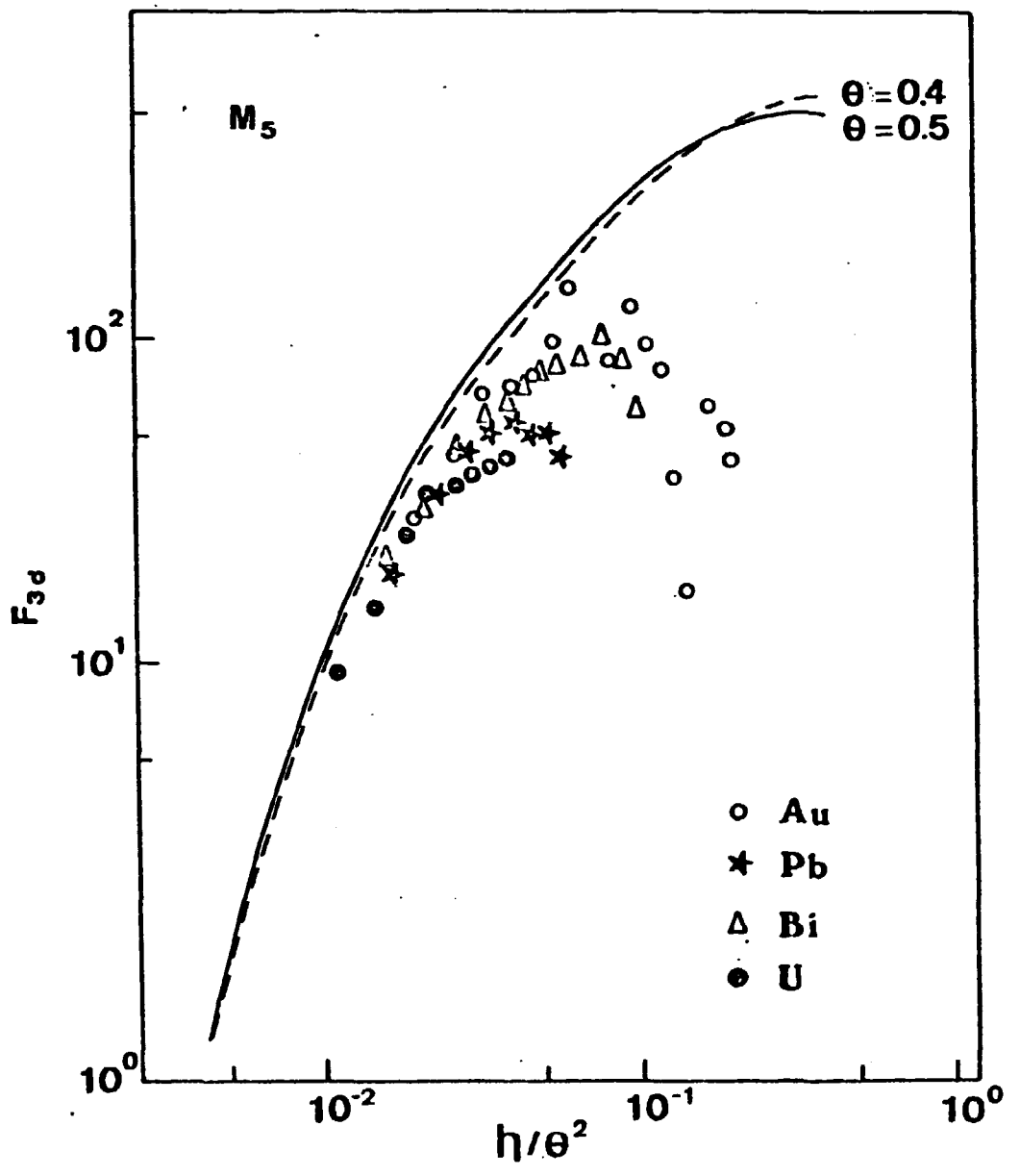

Figure 7

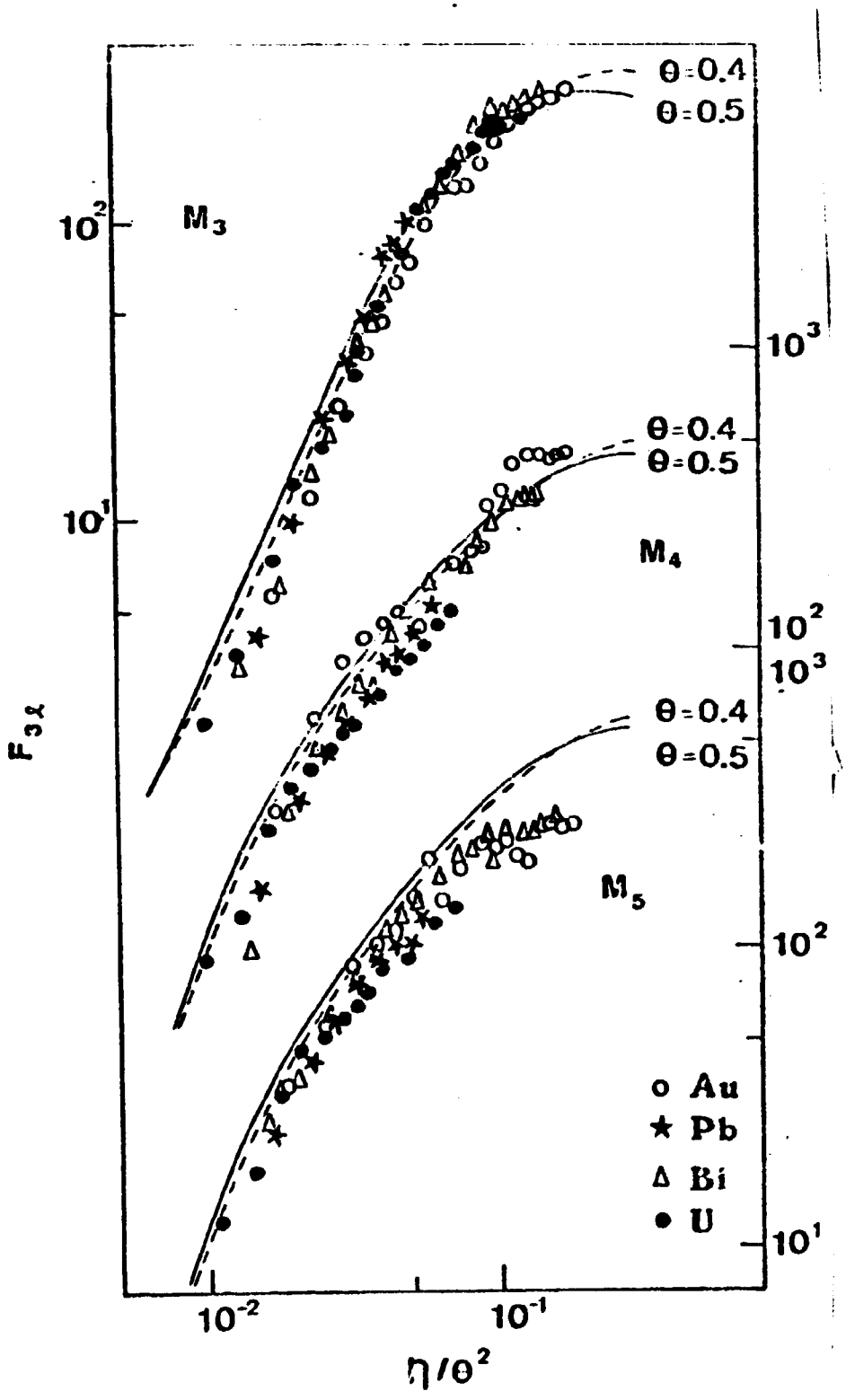
θ=0.4
θ=0.5
M3
10^2
10^1
10^3
θ=0.4
θ=0.5
M4
10^2
10^3
θ=0.4
θ=0.5
M5
10^2
10^1
o Au
★ Pb
Δ Bi
• U
10^-2
10^-1
η/θ^2
F3α

Figure 8